

Article

Geochemistry and Texture of Clinopyroxene Phenocrysts from Paleoproterozoic Picrobasalts, Karelian Craton, Fennoscandian Shield: Records of Magma Mixing Processes

Sergei A. Svetov , Svetlana Y. Chazhengina *  and Alexandra V. Stepanova 

Institute of Geology KarRC RAS, Petrozavodsk 185910, Russia; ssvetov@krc.karelia.ru (S.A.S.); stepanov@krc.karelia.ru (A.V.S.)

* Correspondence: chazhengina@mail.ru

Received: 31 March 2020; Accepted: 9 May 2020; Published: 12 May 2020



Abstract: This paper presents an integrated major and trace element data and crystal size distribution analysis for zoned clinopyroxene phenocrysts hosted in variolitic and massive picrobasalts of the Suisaari Formation, Karelian Craton, Eastern Fennoscandian Shield. Clinopyroxenes in variolitic and massive lavas occur as unzoned, reverse, and normally zoned crystal. Oscillatory-zoned clinopyroxenes are only observed in variolitic lavas. The obtained data were examined in order to evaluate the contribution of magmatic processes such as magma mixing, contamination and fractional crystallization to the formation of various zoning patterns of clinopyroxene phenocrysts. Clinopyroxene phenocrysts in both variolitic and massive lavas originate from similar primary melts from a single magmatic source. The obtained data on composition and texture of clinopyroxene phenocrysts together with the crystal size distribution (CSD) analysis suggest that crystallization of the massive lavas mainly involves fractionation in a closed magmatic system, whereas the crystallization of the variolitic lavas is determined by processes in an open magmatic system. The results provide novel information on the evolution of Paleoproterozoic magmatic systems in the Karelian Craton.

Keywords: clinopyroxene phenocryst; zoning; variolitic lava; magma mixing processes

1. Introduction

Pyroxenes are abundant rock-forming minerals in volcanic rocks. They exhibit diverse varieties of textural, zoning and compositional features that record the crystallization history of magma from early crystallization (where pyroxenes form large phenocrysts) to the final stage (in which pyroxene microcrysts crystallize in the groundmass) [1–3]. Therefore, the chemical composition and texture of pyroxenes from volcanic rocks are usually used as the markers of the evolution of magma composition during crystallization in open and closed magmatic systems. Additionally, compositional and textural characteristics of pyroxenes can provide information on the physicochemical conditions of crystallization including temperature, pressure, and oxygen fugacity variations during the evolution of magmatic systems [4–6]. Furthermore, pyroxenes are more resistant to metamorphic alterations under greenschist facies compared to olivine, which provides the possibility of their use as petrogenic indicators for a wide compositional range of volcanic rocks.

Pyroxenes have been intensively studied worldwide over the past 40 years. Numerous studies of pyroxenes from geochemically diverse volcanic rocks of various geodynamic settings [2,7–12] have demonstrated that their composition and texture are reliable indicators by which to estimate the evolution and ascent histories of magmas. This approach has been successfully applied to decipher the

evolution of modern volcanic systems [13–15] as well as Mesozoic–Paleozoic paleovolcanic series of volcanic rocks [16–18].

In the Paleoproterozoic picrobasalts of the Suisaari Fm, Ludikovian, Onega Basin of the Karelian Craton in the Eastern Fennoscandian Shield, clinopyroxene is an ubiquitous mineral. The most intriguing feature of Suisaari basalts is a wide occurrence of variolitic lavas described by F. Yu. Levinson-Lessing more than 100 years ago [19]. The origin of variolitic lavas has been an intensively debated problem over the last 40 years [20–28]. Yalguba variolitic lava origin models have included liquation [19–23], mixing of felsic and mafic magmas [24,25], quenching crystallization from a strongly overheated melt [26,27] and low-temperature secondary alterations of basic rocks [28]. Despite intensive study, several questions (including the crystallization mechanism and role of magma mixing and contamination by crustal material in variolitic texture formation) remain unresolved. Clinopyroxenes that are abundant in all Suisaari Fm lavas could give insight into the origin of mafic melts and their crustal evolution, including fractional crystallization, contamination by crustal materials and magma system evolution. Since clinopyroxenes from volcanic rocks of Suisaari Fm exhibit a wide range of compositional, zoning and textural patterns [29], the study of their major and trace element compositions and textures provides the opportunity to decipher the petrogenesis of host picrobasalts.

This paper presents the integrated major and trace element data and a crystal size distribution analysis for zoned clinopyroxene phenocrysts hosted in variolitic and massive picrobasalts of Suisaari Fm. The obtained data were examined in order to evaluate the contribution of magmatic processes such as magma mixing, contamination and fractional crystallization to the formation of various zoning patterns of clinopyroxene phenocrysts. The results provide novel information on the evolution of Paleoproterozoic magmatic systems in the Karelian Craton.

2. Geological Setting

The Yalguba Ridge is located in the central part of the Paleoproterozoic Onega Basin, in the southeastern part of the Archaean Karelian craton, Fennoscandian Shield [30,31] (Figure 1). The Yalguba Ridge locality belongs to the Suisaari Fm of the Ludikovian (approx. 2.0 Ga) volcanic-sedimentary succession of the Middle Paleoproterozoic. Suisaari Fm occurs mainly in the western part of the Onega Basin within an area of approximately 2000 km² and comprises mostly mafic-ultramafic (picritic and picrobasaltic) volcanic rocks [31]. The total thickness of Suisaari Fm does not exceed 420 m and is dominated by lavas (75 vol.%) compared with volcano-sedimentary rocks with widespread pyroclastic products (25 vol.%) [31,32]. A depositional age of the Suisaari Fm is constrained by the Sm-Nd mineral isochron age of 1975 ± 24 Ma obtained for the Konchezero gabbro-peridotite sill that is coeval to Suisaarian mafic lavas [33].

Subvolcanic rocks that are co-magmatic with the lavas from Suisaari Fm are represented by dolerite and peridotite dykes and sills. The Yalguba Ridge section represents the upper part of the Suisaari Formation and is represented by massive, pillowed and variolitic mafic lavas interbedded with tuffs with thickness up to 3 m. The rocks are altered from the prehnite-pumpellyite to greenschist facies. Detailed petrography has been described in [22,31,32,34].

In the Yalguba Ridge locality, mafic lavas can have a thickness of up to 16 m and have a specific variolitic structure defined by globules (varioles) with diameters varying from 0.1 to 8 mm (Figure 2). These are composed of pyroxene phenocrysts and microcrysts that are embedded in fine-grained groundmass, with needle-shaped pyroxene and plagioclase microlites as well as quartz. Globules commonly have feldspar rims. Matrices (spaces between globules) contain pyroxene phenocrysts and microcrysts embedded in augite–actinolite–chlorite groundmass (Figure 2c). The variolitic lavas are composed (in a modal percentage) of 30–40% albite-rich plagioclase (Ab₁₀₀₋₈₇), 30–40% clinopyroxene, minor quartz together with feldspar, chromite, secondary chlorite and epidote. The massive lavas are characterized by a fine-grained ophitic texture with pyroxene phenocrysts and microcrysts embedded in pyroxene-plagioclase-quartz groundmass. The massive lavas contain 30–35% clinopyroxene, 25–30% plagioclase, minor quartz together with feldspar, chromite, secondary epidote, chlorite and carbonates.

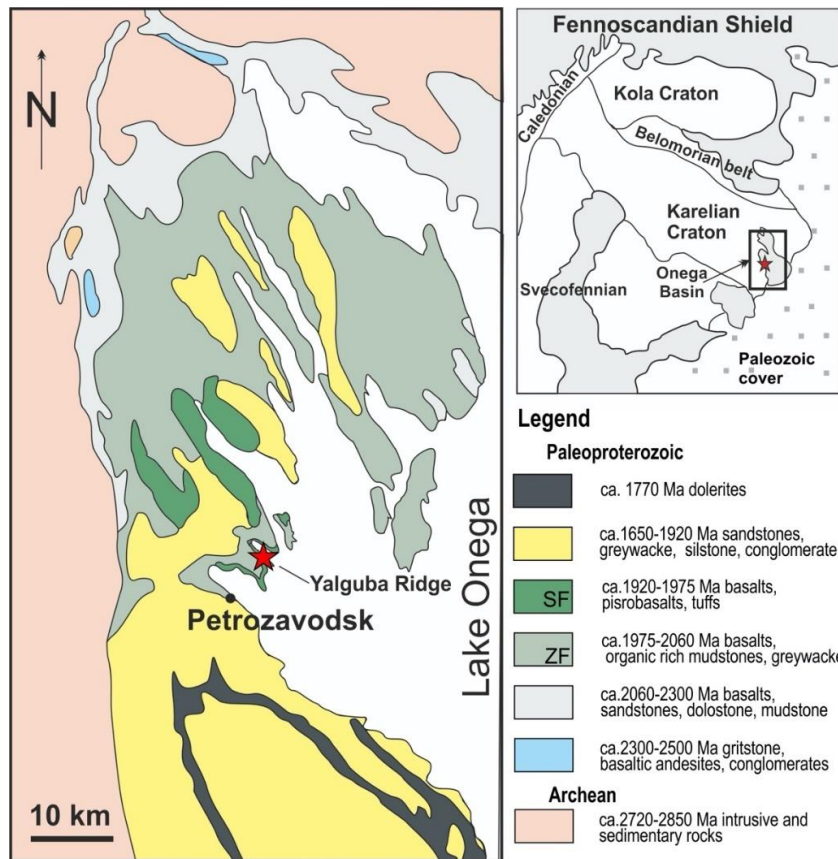


Figure 1. Schematic geological map of the western part of the Onega Basin and sampling locations. Modified from [33]. SF—Suisaari Formation; ZF—Zaonega Fm; asterisk marks the sampling area. Reproduced with permission from Kulikov V.S., Contributions to Mineralogy and Petrology; published by Springer-Verlag, 1998.

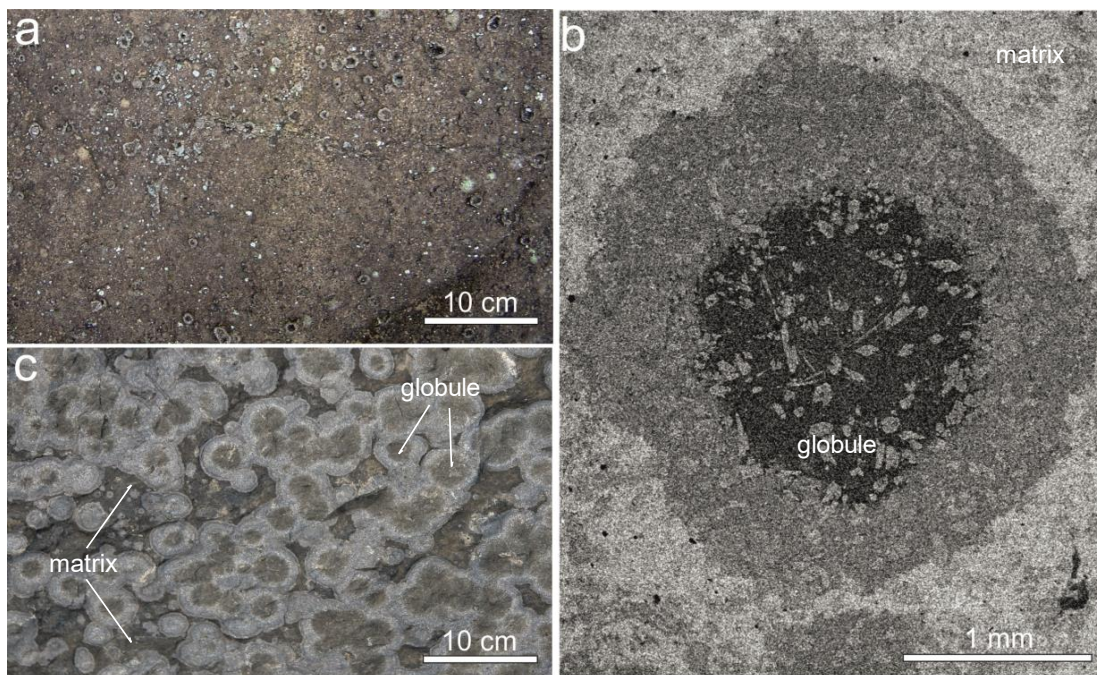


Figure 2. Representative field photographs of the massive (a) and variolitic (b) lavas and a backscattering electron image of a globule from the variolitic lava (c).

The globules of variolitic lavas are enriched in SiO₂ 54–66%, MgO 6–12 wt.% and alkalis (Na₂O + K₂O up to 7 wt.%), and can be classified as andesites and dacites [22,23,34]. It should be noted that the inner part of a globule is enriched in Na₂O (up to 8 wt.%) and outer rim of the globule is enriched in K₂O (up to 14 wt.%) [23]. The matrices of variolitic lavas correspond to picobasalts and contains 43–46 wt.% of SiO₂ and 13–17 wt.% of MgO. The massive lavas are a basalt with 47 wt.% of SiO₂, 7 wt.% of MgO enriched in TiO₂ (1.65 wt.%) and alkalis (Na₂O+K₂O up to 6 wt.%) (Table S1).

3. Sampling and Methods

Twenty samples of variolitic lavas and 10 samples of massive lavas were collected from outcrops of the Yalguba Ridge. Sampling was undertaken across variolitic lava sequences with a thickness of 16 m and an underlying massive lava flow with a thickness of 10 m. The major element composition of clinopyroxene from 20 thin sections was studied by energy-dispersive spectroscopic (EDS) analyses, and trace element compositions of clinopyroxene phenocrysts from four thin sections were analyzed by secondary ion mass spectrometry.

Clinopyroxene phenocrysts were detected in the variolitic lava both in globules and matrices, as well as in the massive lavas. The phenocryst content was low and clinopyroxene phenocrysts were more abundant in the variolitic than in the massive lavas. All samples of the variolitic lavas contained clinopyroxene phenocrysts, whereas these were observed in only two out of 10 samples of the massive lavas. All clinopyroxene phenocrysts were well-preserved and showed no secondary alteration, with the exception of phenocrysts from the matrices of variolitic lavas, which exhibited signs of chloritization.

Major and minor element compositions and textural features of clinopyroxenes were analyzed using a VEGA II LSH (Tescan, Brno, Czech Republic) scanning electron microscope coupled with an INCA Energy 350 energy dispersive detector at the Centre for Collective Usage, Karelian Research Centre, RAS (Petrozavodsk, Russia). The analyses were performed on polished thin sections under the following analytical conditions: W cathode, 20 kV accelerating voltage, 20 nA beam current, 2 µm beam diameter, counting time of 90 s. The accuracy of analyses was better than 1% for the major elements and 5% for the minor elements.

Based on the backscattering electron (BSE) imaging and EDS analysis, a set of representative clinopyroxenes with various zoning patterns were selected for trace element analysis using secondary ion mass spectrometry techniques. Concentrations of minor elements for these samples were determined using a Cameca IMS 4f secondary ion mass spectrometer (Cameca, Gennevilliers, France) at the Yaroslavl Branch of the Physicotechnical Institute of RAS following the analytical procedure in [17]. The concentration uncertainties were determined to be 5–10% at concentrations >1 ppm, and up to 20% at concentrations of 0.1–1 ppm.

Crystal size distribution (CSD) analysis was carried out on the thin section BSE images of the variolitic and massive lavas using the ImageJ software. Clinopyroxene grains were isolated by threshold filters from feldspar and groundmass and manually vectorized to define the grain boundaries. Grains smaller than 10 pixels and grain fragments in the image edges were eliminated from the analysis. CSD statistics were calculated for 698 clinopyroxene grains from the globules, 298 grains from the variolitic lava matrix and 434 grains in the massive lavas. Crystal parameters such as length, width, area, centroid, and fit ellipse were determined using the Image J software in order to characterize the clinopyroxene morphology. CSD correction software [35] was used to calculate 3D parameters from 2D section data. CSD data are listed in Supplementary Materials Table S2.

4. Results

Major element composition data obtained for 350 clinopyroxenes, including phenocrysts and microcrysts from the variolitic and massive lavas of the Yalguba Ridge, indicated that they all corresponded to augite [36], with En content ranging from 31% to 52%.

Clinopyroxenes were present in the variolitic and massive lavas as zoned and unzoned phenocrysts (>100 µm); euhedral, tabular, or prismatic microcrysts (10–50 µm); and groundmass acicular microlites

(<10 μm), intergrown with plagioclase. According to the zoning patterns, clinopyroxene phenocrysts were categorized into four groups: normal-zoned with Mg-rich cores; reverse-zoned with Mg-poor cores; oscillatory-zoned with an Mg-poor core, Mg-rich mantle, and Mg-poor rim; and “homogenous” (unzoned) clinopyroxenes (Figure 3). In the variolitic lavas, “homogenous” (unzoned) normal and reverse-zoned clinopyroxenes were recognized both in globules and matrices, whereas the oscillatory-zoned clinopyroxenes were identified only in globules. No distinct differences in texture and chemical composition were recorded for the clinopyroxenes from globules and matrices (Table 1).

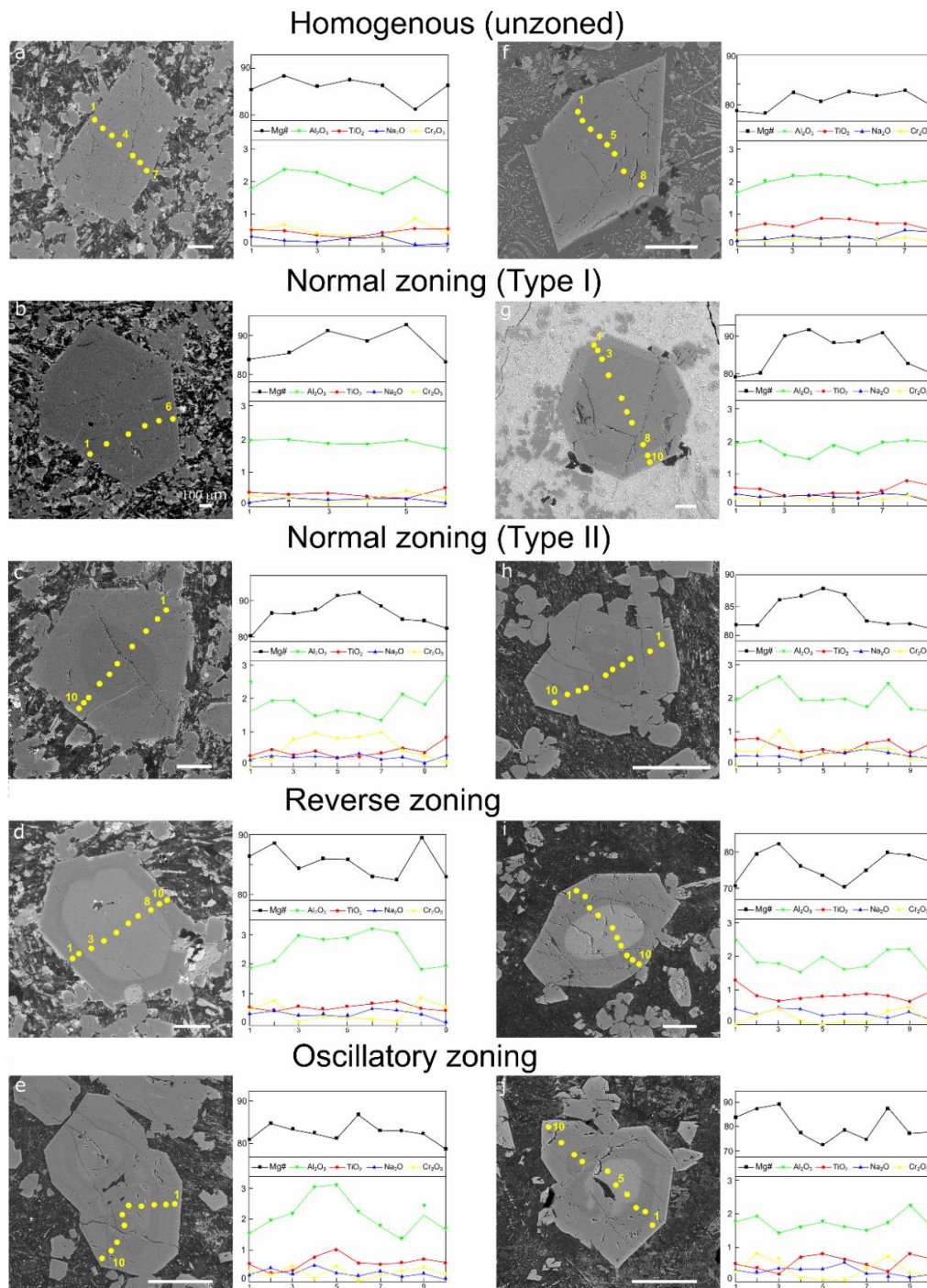


Figure 3. Representative BSE images and analytical points with major element compositions for clinopyroxene phenocrysts from the massive (a–d) and variolitic (e–j) lavas with various zoning patterns. Scale bar corresponds to 100 μm. The yellow dots mark the single point EDS analysis.

Table 1. Summary of zoning patterns, textures, and chemical characteristics of clinopyroxene phenocrysts from the variolitic and massive lavas of Yalguba Ridge. Notes: n—total number of phenocrysts; g—globule; m—matrix; ΣREE—total concentration of rare earth elements.

Zoning	Texture	Content (%)		Mg#				ΣREE, ppm			
		Variolitic (n = 30)	Massive (n = 10)	Core		Rims		Core		Rims	
				Variolitic	Massive	Variolitic	Massive	Variolitic	Massive	Variolitic	Massive
Homogenous (HP)		33	70	86–88 (g) 81–83 (m)	90–92	80–83 (g) 78–80 (m)	80–82	13 (g) 27 (m)	30	21 (g) 29 (m)	27
Normal type I (NZ I type)		30	10	90–93 (g) 88–92 (m)	85–92	79–86 (g) 79–83 (m)	80–86	35 (g) 13 (m)	21	45 (g) 33 (m)	29
Normal type II (NZ II type)		10	10	86–88 (g)	87–90	82–84 (g)	83–85	54 (g)	14	89	26
Reverse (RZ)		20	10	68–73 (g) 70–75 (m)	82–84	79–82 (g) 81–84 (m)	86–89	137 (g) 117 (m)	42	66 (g) 64 (m)	27
Oscillatory (OZ)		7	-	73–84 (g) mantle: 83–89 (g)	-	75–84 (g)	-	114 (g) mantle: 26 (g)	-	47 (g)	-

4.1. Major Element Content and Zoning Patterns

“Homogenous” clinopyroxene phenocrysts (HP type) occurred both in variolitic and massive lavas as euhedral to subhedral grains with a size of 400–700 μm . They had no signs of zoning both in polarizing light and BSE (Figure 3a,f). The amount of “homogenous” clinopyroxene phenocrysts was less than 30% in the variolitic lavas, and 70% in the massive lavas. In the variolitic lavas, HP were characterized by the gradual decreasing of the Mg# ($\text{Mg\#} = 100 \times \text{Mg}/(\text{Mg} + \text{Fe})$ in mole considering all iron as Fe^{2+}) values from 83–88 in the central parts of the grains to 78–83 in their margins. In the massive lavas, Mg# of HP gradually decreased from 90–92 in the central parts of the grains to 80–82 in their margins (Table 1). The decreasing of Mg# was coupled with increasing TiO_2 content and decreasing Cr_2O_3 in both types of lavas. Chemical trends within center-to-margin profiles of HP clinopyroxenes were similar to that of normal-zoned clinopyroxenes.

Clinopyroxene phenocrysts with normal zoning (NZ) also occurred in the variolitic and massive lavas. These were characterized by the presence of a high-Mg core in the central part of the grain. The core was mantled by a rim that could be well-recognized in BSE (Figure 3b,g). Clinopyroxene phenocrysts with normal zoning can be divided into two subgroups. Type I normal zoning clinopyroxene phenocrysts (NZ Type I) were represented by relatively large (400–1000 μm) euhedral to subhedral clinopyroxenes that occurred both in variolitic and massive lavas. The NZ Type I phenocrysts had a euhedral core surrounded by a thin rim with sharp interfaces between zones. The core/rim thickness ratio was 10:1 (Figure 3b,g). The zoning is defined by the contrast differences in major element contents. In the variolitic lavas, the Mg# decreased from 88–93 in the core to 79–86 in the rims (Table 1). In the massive lavas, Mg# values decreased from 85–92 in the cores to 80–86 in the rims. The variation of Mg# with TiO_2 and Cr_2O_3 was also observed in the variolitic and massive lavas such that Cr_2O_3 slightly decreased and TiO_2 slightly increased within declining Mg# (Figure 4, Table S3).

Type II of normal-zoning phenocrysts (NZ Type II) was represented by clinopyroxenes with relatively small (200–300 μm) grain sizes. This sub-type of normal-zoning phenocryst is characterized by a presence of rounded cores enriched in MgO (Figure 3c,h) and thick rims with a core-to-rim thickness ratio of ~1:1. The trends of core-to-rim compositional changes were similar to those of NZ Type I clinopyroxenes (Table 1). It should be noted that cores of NZ Type II phenocrysts in the massive lavas were characterized by high Cr_2O_3 contents up to 1.4 wt.% (Figure 4). The major element chemistry of the high-Cr cores was indistinguishable from the other high-Mg pyroxenes. The amount of normal-zoned clinopyroxene phenocrysts was higher in the variolitic lavas (40%) than in the massive lavas (20%). Moreover, in the variolitic lavas, NZ Type I was more abundant, forming up to 30% of phenocrysts compared to NZ Type II (10%).

Reverse-zoned clinopyroxenes (RZ type) formed subhedral 200–250 μm grains. They were less abundant in the variolitic (20%) and massive (10%) lavas compared with the NZ phenocrysts. The RZ phenocrysts usually have rounded cores surrounded by a rim that can be well recognized in the BSE images (Figure 3d,i). The core-to-rim thickness ratios varied from 10:1 in the massive lavas to 1:1 in the variolitic lavas. The RZ phenocrysts in the variolitic and massive lavas had Mg-poor cores but different Mg# values. In the massive lavas the cores of the RZ type phenocrysts had an Mg# = 82–84, and in the variolitic lavas Mg# values were 68–75 (Table 1). The rims in RZ grains were more magnesian than the cores both in the massive (Mg# = 86–89) and variolitic (Mg# = 79–84) lavas. The Mg# values in the RZ clinopyroxenes coincided with Mg# values in the rims of normal-zoned clinopyroxene phenocrysts (Figure 4). In contrast with the normal-zoned clinopyroxenes, the cores of RZ clinopyroxenes had lower Cr_2O_3 contents and have higher TiO_2 contents compared to the rims. The Al_2O_3 and Na_2O contents showed narrow core-to-rim variations with no relation to the variations in Mg# (Figure 4).

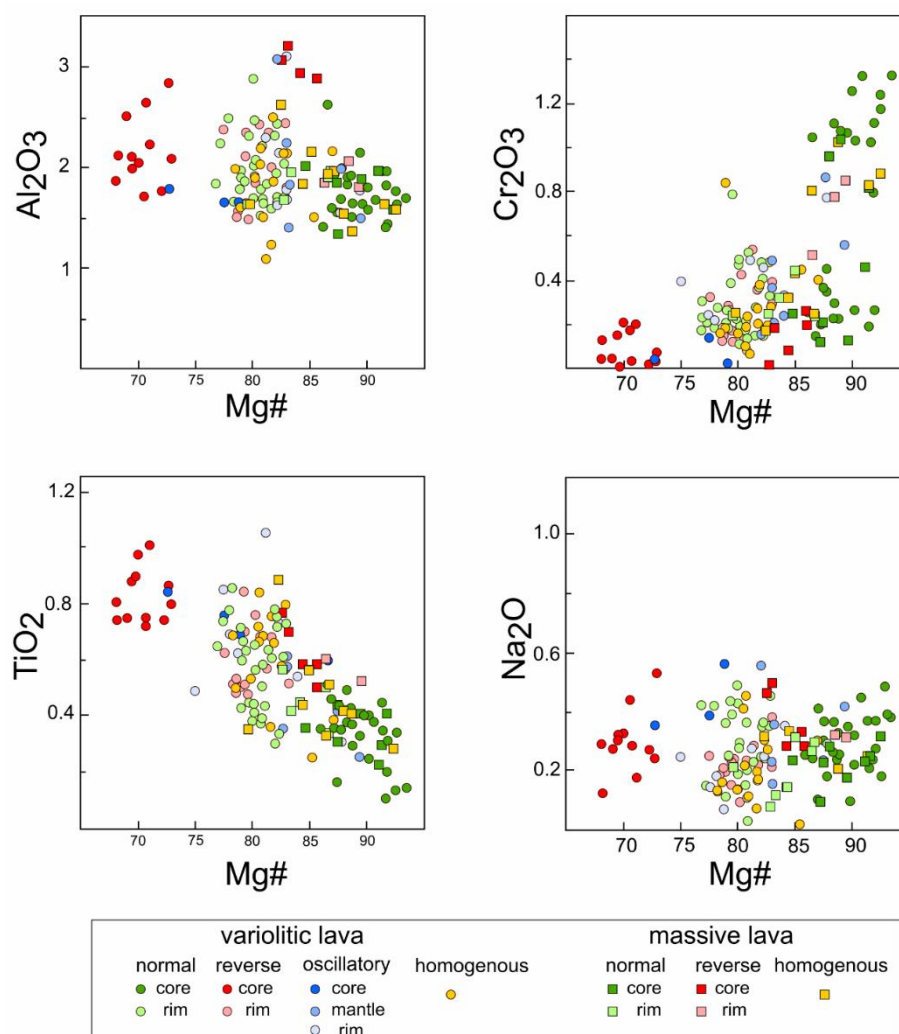


Figure 4. Compositional variations of clinopyroxene phenocrysts from the variolitic and massive lavas of the Yalguba Ridge in terms of Mg# vs. Al_2O_3 , Cr_2O_3 , TiO_2 and Na_2O (concentration in wt.%).

Oscillatory-zoned clinopyroxenes (OZ type) were identified only in the variolitic lavas and were the most rare phenocryst type, forming less than 10% of phenocrysts. They commonly had a subhedral morphology with rounded cores (~20–30 μm) surrounded by euhedral layers with sharp boundaries characterized by a thickness of approximately 15–30 μm (Figure 3e,j). Oscillatory zoning is defined by Mg-poor cores (Mg# = 73–84), relatively Mg-rich mantles (Mg# = 83–89), and Mg-poor rims (Mg# = 75–84) (Figure 4, Table 1). The cores had high TiO_2 and low Cr_2O_3 contents compared with the mantles and rims. The TiO_2 content decreased in the mantles and slightly increased in the rims, whereas the Cr_2O_3 content was relatively constant in the mantles and rims.

4.2. Trace Element Composition of Clinopyroxene Phenocrysts

Cores and rims of zoned clinopyroxenes had various rare earth element (REE) contents depending on the zoning type, but were all characterized by similar convex upward REE distribution patterns with minor negative Eu anomalies. Compositional similarity was also pronounced in the trace element distribution characterized by the depletion in high field strength elements (HFSEs) (Figure 5).

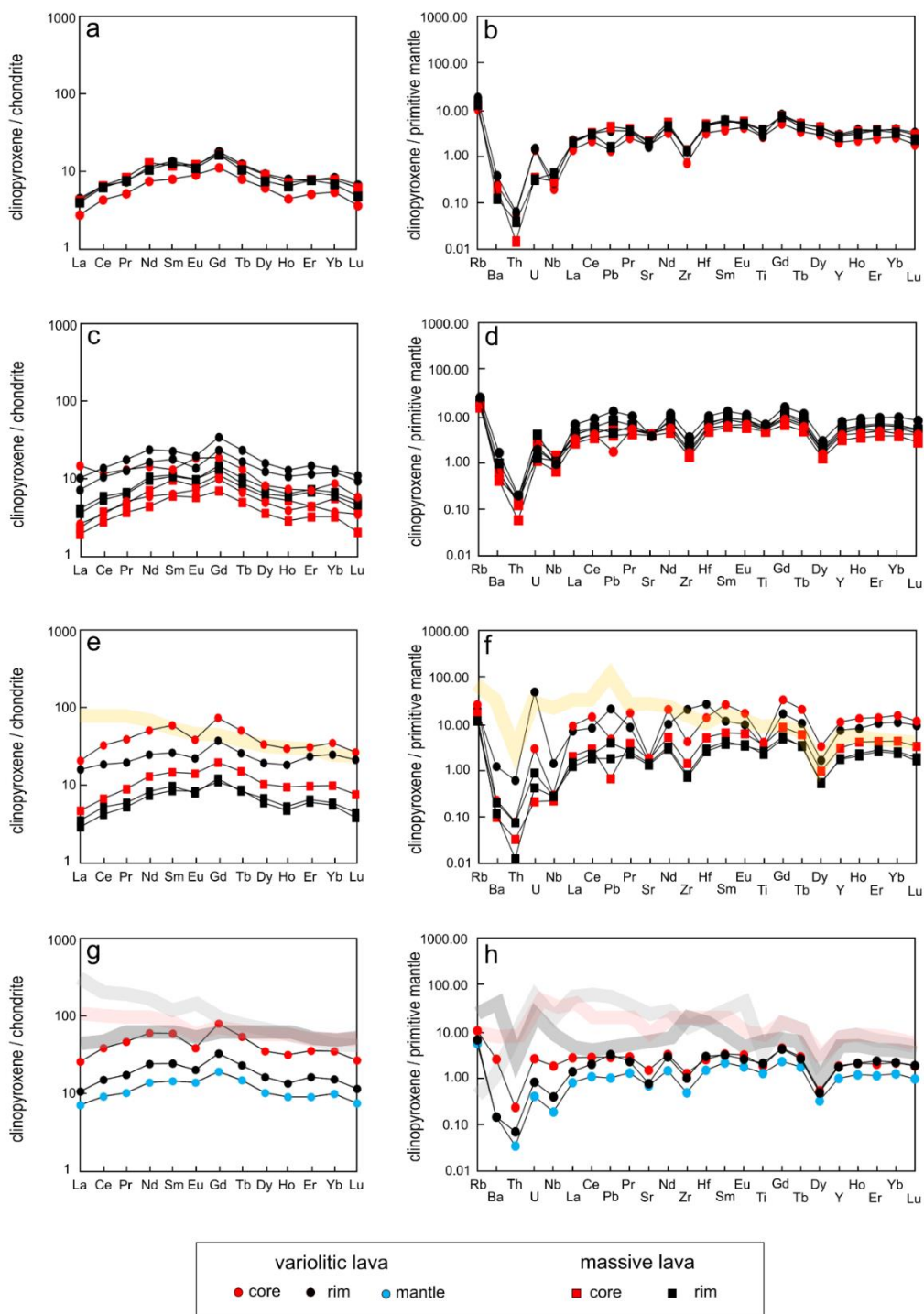


Figure 5. Chondrite-normalized REE distribution patterns and primitive mantle-normalized trace element distribution patterns for clinopyroxene phenocrysts from the variolitic and massive lavas with homogeneous patterns (HP) (a,b), normal zoning (NZ) (c,d), reverse zoning (RZ) (e,f), and oscillatory zoning (OZ) (g,h). The normalization values are from [37]. The whole-rock composition of the massive lavas (yellow colored line) is shown in e and f. The whole-rock composition of the variolitic lavas (dark grey color for matrix Type I, light grey color for matrix Type II, and rose color for the globule composition) is shown in (g,h) (modified from [34]).

HP type phenocrysts were characterized by convex upward REE distribution patterns with $\Sigma\text{REE} = 13\text{--}30$ ppm, depletion in both LREE (light rare earth elements), heavy rare earth elements (HREE)

([La/Sm]_n = 0.33–0.37, [Gd/Yb]_n = 2.05–2.30), and minor negative Eu anomalies (Eu/Eu* = 0.76–0.78) (Eu/Eu* = Eu_N/(Sm_N + Gd_N)^{1/2}) (Figure 5a). The REE content showed no significant variations along the crystal profile. HP type phenocrysts were characterized by a depletion of HFSEs with negative Nb and Zr anomalies. Nb/Nb* varied from 0.23 in the variolitic lavas to 0.51 in the massive lavas. The central parts of HP phenocrysts showed no significant Pb anomalies, whereas the margins of the grains showed slightly negative Pb anomalies (Figure 5b).

In the NZ type phenocrysts, rims were enriched in REE (ΣREE = 33–89 ppm) compared to the cores (ΣREE = 13–54 ppm). Clinopyroxene cores and rims exhibited similar convex upward REE distribution patterns with depletions of both LREE and HREE ([La/Sm]_n = 0.38–0.42, [Gd/Yb]_n = 1.93–2.59) (Figure 5c). The NZ type phenocrysts showed slightly negative Eu anomalies (Eu/Eu* = 0.69–0.89). NZ cores of clinopyroxenes from both variolitic and massive lavas were depleted in HFSEs with positive Nb anomalies (Nb/Nb* = 1.12–1.39). In contrast to the cores, the rims of NZ clinopyroxenes exhibited HFSE depletion with negative Nb anomalies (Nb/Nb* = 0.25–0.49). Additionally, the cores had slightly negative Pb anomalies, whereas the rims exhibited no significant Pb anomalies (Figure 5d).

The RZ type clinopyroxenes from the variolitic lavas had higher REE content compared to that of the massive lavas, which decreased from ΣREE = 117–137 ppm in the cores to ΣREE = 64–66 ppm in the rims. The reverse-zoned clinopyroxenes from the massive lavas had lower REE content but exhibited a similar trend of decreasing REE content from the cores (ΣREE = 42 ppm) to the rims (ΣREE = 27 ppm). The REE distribution patterns in the cores and rims of RZ clinopyroxenes resembled the convex upward REE distribution patterns of homogeneous and normal-zoned clinopyroxenes ([La/Sm]_n = 0.31–0.35, [Gd/Yb]_n = 2.01–2.09) (Figure 5e). The RZ clinopyroxenes from the variolitic lavas showed more-pronounced negative Eu anomalies (Eu/Eu* = 0.58–0.72) than clinopyroxenes, with the same zoning patterns from the massive lavas (Eu/Eu* = 0.72–0.86). RZ clinopyroxene cores and rims were depleted in HFSEs, with negative Nb and Zr anomalies (Figure 5f). Nb/Nb* varied from 0.11 to 0.22 within the core-to-rim profiles in the variolitic lavas. The cores and rims of RZ clinopyroxenes from the massive lavas exhibited no variation in Nb/Nb* values, which ranged from 0.28 in the cores to 0.27 in the rims. Similar to NZ clinopyroxenes, the cores of RZ phenocrysts also had slightly negative Pb anomalies. The rims of RZ clinopyroxenes from the variolitic lavas showed some distinctive features including positive U anomalies and the absence of negative Zr anomalies.

The cores of oscillatory-zoned (OZ type) clinopyroxenes had higher REE concentrations (ΣREE = 114 ppm) compared with the mantles (ΣREE = 26 ppm), whereas the rims exhibited intermediate values (ΣREE = 47 ppm). Cores, mantles, and rims were characterized by similar convex upward REE distribution patterns ([La/Sm]_n = 0.35–0.40, [Gd/Yb]_n = 1.94–2.09), which resembled the REE distribution patterns of normal and reverse-zoned clinopyroxenes (Figure 5g). OZ clinopyroxenes were depleted in HFSEs, with negative Nb and Zr anomalies (Figure 5h). OZ mantles were characterized by higher values of Nb/Nb* = 0.45 compared to the OZ cores and rims (Nb/Nb* = 0.28 and 0.31, respectively).

4.3. Crystal Size Distribution of Clinopyroxenes

The analyses of crystal size distributions (CSDs) are becoming increasingly used to study the crystallization kinetics of magmatic systems [12,38,39]. The CSD results obtained for clinopyroxenes from the variolitic and massive lavas of the Yalguba Ridge are plotted on a population density (ln(n), μm⁻⁴) vs crystal size (L, μm) diagram. Figure 6 shows that clinopyroxene from the variolitic lavas had inverse relationships between grain length and population density. CSD curves of clinopyroxenes in the globules and matrices of the variolitic lavas were characterized by kinked linear trends marking two size crystal populations. The CSD curves of these clinopyroxenes showed linear trends with a slope of −0.06 for a crystal size smaller than 120 μm, and −0.03 for a crystal size larger than 120 μm. In contrast, the CSD curves of clinopyroxenes from the massive lavas exhibited a concave-downward CSD at sizes smaller than 20 μm (Figure 6) and a linear trend with a slope of −0.05 at a crystal size larger than 20 μm.

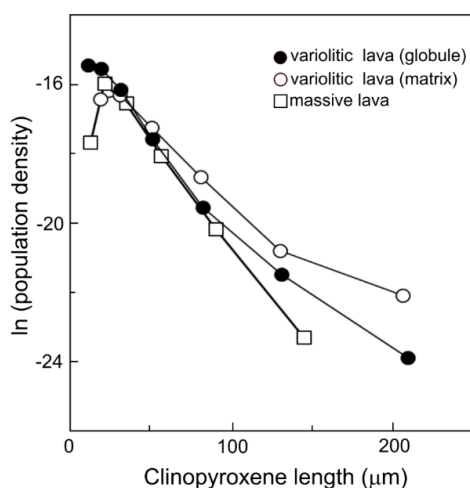


Figure 6. Crystal size distribution (CSD) of clinopyroxene crystals from of the variolitic (globule and matrix) and massive lavas from the Yalguba Ridge.

To estimate the grain size, an equivalent circle diameter (ECD) was calculated from the measured surface area that corresponded to the diameter of a circle with an area equivalent to the crystal area. Clinopyroxenes both from the variolitic and massive lavas were characterized by an ECD lower than 100 μm with maximum size values between 25–40 μm. The aspect ratio (major-axis length/minor-axis length of the best fit ellipse) of clinopyroxenes from both variolitic and massive lavas (AR, defined as AR = major axis length/minor axis length of the best fit ellipse) were also comparable, varying from 1 to 3. Moreover, there was similarity in the 2D orientation, evidenced by the similar values of alignment factors (AFs) for the samples from the variolitic (AF = 0.06) and massive (AF = 0.10) lavas. The low values of AFs reflected a lack of specific orientation. It should be mentioned that the studied samples were not oriented, so the measured 2D orientations were relative.

5. Discussion

The variolitic and massive lavas of the Yalguba Ridge belong to the Suasaari Fm of the Onega Basin, which represents a continental flood basalt province in the Fennoscandian Shield. Previous lithostratigraphic, chemical, and isotope studies [33,34] have revealed that the volcanic rocks of the Onega Basin originated from a single mantle plume. The uppermost Onega Basin volcanic series (including the Suisaari Fm) have compositional features comparable with the modern oceanic plume-derived magmas, including high MgO contents, enrichment in Ti and other HFSEs, and differentiated REE patterns. These features indicate the origin of Suisaarian primary melts may have been due to a deep-seated mantle melting caused by the mantle plume rising [33]. In contrast to high-Mg Suisaarian basalts, low-Mg ones have shown signs of contamination and fractional crystallization characterized by enrichment in SiO₂ and depletion of MgO and HFSE. The available geochemical, isotopic, and geochronological data indicate that generation of approximately 1.96–1.97 Ga occurred within several short pulses of melting caused by the mantle plume rising [33,40–42]. These pulses contaminated a variety of high- and low-Mg mafic rocks in various proportions.

The origin of the variolitic texture in volcanic rocks has been studied for a long time, but is still debated. Since clinopyroxene is a ubiquitous mineral in the lavas of the Yalguba Ridge, we used it as a petrogenetic indicator to decipher the key stages in the magma system evolution in order to clarify the differences in crystallization history of the variolitic and massive lavas.

The evolution of magmatic systems involves complicated processes such as fractional crystallization, magma mixing, and contamination by crustal materials that might be recorded in the compositional and textural features of pyroxenes. Three general groups of pyroxene populations are commonly classified in magmatic systems [39,43] including autocrysts, antecrysts, and xenocrysts. Autocrysts crystallized from the final melt, which corresponded to the whole-rock compositions of

the host rocks. Antecrysts are introduced in the magma, in which they are now hosted, through different magma replenishment events or via magma convection, whereas xenocrysts are incorporated as a result of contamination. Since autocrysts are the only crystal in equilibrium with their host's whole-rock composition, they can be distinguished from antecrysts or xenocrysts by evaluating for chemical equilibrium.

5.1. Clinopyroxene—Melt Equilibrium

The equilibrium between clinopyroxene and melt represented by whole-rock composition of the variolitic and massive lavas was tested using the partition coefficient of Fe-Mg between clinopyroxene and melt, which has been estimated to be $K_{d_{Fe-Mg}} = 0.275 \pm 0.067$ [44]. Figure 7 shows that in massive lavas, the margins of several HP clinopyroxenes ($K_{d_{Fe-Mg}} = 0.19$ – 0.29) and rims of the NZ ($K_{d_{Fe-Mg}} = 0.21$ – 0.24) and OZ ($K_{d_{Fe-Mg}} = 0.20$ – 0.25) clinopyroxenes were in equilibrium with their host rock compositions at $Mg\# = 0.52$. The cores of OZ clinopyroxenes slightly deviated from the equilibrium ($K_{d_{Fe-Mg}} = 0.30$ – 0.32) and appeared to crystallize from the calculated equilibrium melt, with $Mg\# = 0.48$ – 0.49 . The NZ cores showed more distinct deviations ($K_{d_{Fe-Mg}} = 0.14$ – 0.16) from the equilibrium, and should have crystallized from the melt at $Mg\# = 0.60$ – 0.68 , which is higher than the $Mg\#$ of host massive lavas. In general, the compositions of clinopyroxene phenocrysts from the massive lavas appeared to be close to equilibrium compared with the clinopyroxene phenocrysts from the variolitic lavas. Similar to the massive lavas, the margins of several HP clinopyroxenes from the variolitic lavas also exhibited the equilibrium features ($K_{d_{Fe-Mg}} = 0.28$ – 0.44) with their host rock composition at $Mg\# = 0.59$. In contrast with the massive lavas, the rims of NZ, RZ, and OZ clinopyroxenes from the variolitic lavas showed disequilibrium features ($K_{d_{Fe-Mg}} = 0.35$ – 0.42) and were calculated to be in equilibrium with a melt at $Mg\# = 0.48$ – 0.53 . Additionally, several cores of NZ clinopyroxenes were in equilibrium with the whole-rock composition ($K_{d_{Fe-Mg}} = 0.17$ – 0.28), whereas the cores of RZ and OZ clinopyroxenes exhibited strong deviations from the equilibrium ($K_{d_{Fe-Mg}} = 0.61$ – 0.80). The $Mg\#$ of melts, which should have been in equilibrium with the cores of RZ and OZ clinopyroxenes from the variolitic lavas, were calculated to be $Mg\# = 0.35$ – 0.38 and $Mg\# = 0.40$ – 0.50 , respectively. Since the $K_{d_{Fe-Mg}}$ values of the cores from RZ and OZ clinopyroxenes were the furthest from the equilibrium value, they could be interpreted as the antecrysts crystallized from the early batch of magmas or xenocrysts, which are foreign to the magma system.

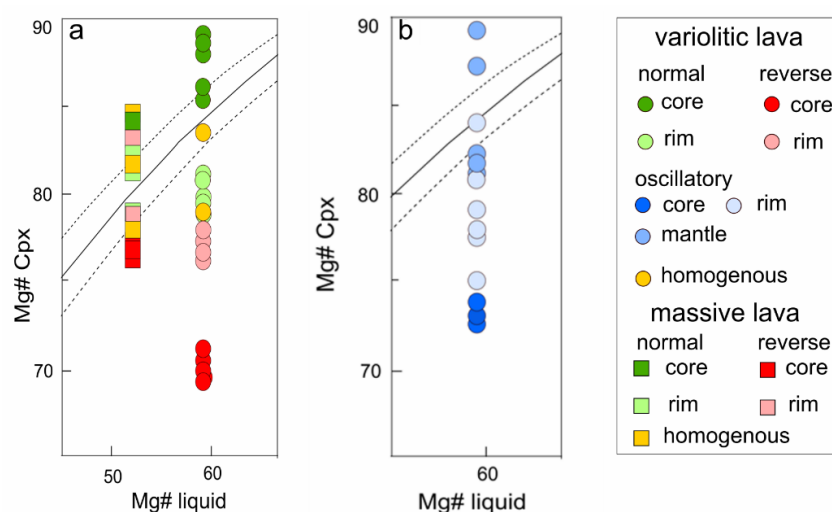


Figure 7. Mineral-melt equilibrium diagrams [44] for clinopyroxene phenocrysts from the variolitic and massive lavas of the Yalguba Ridge with various zoning patterns: normal, reverse, and homogeneous (a) and oscillatory for clinopyroxene phenocrysts from variolitic lava (b). Dashed curves represent a 2σ variation (± 0.3) of the equilibrium value; the equilibrium value of $K_{d_{Fe-Mg}} = 0.275 \pm 0.067$ [44] is marked by the solid curve.

A clinopyroxene-only pressure independent thermometer [45] was used to calculate the temperatures of crystallization for the clinopyroxenes, which were determined to be in equilibrium with the host's whole-rock composition. The temperatures of the clinopyroxenes from the variolitic lavas were determined to be 1192 ± 26 °C, which is similar to the crystallization temperature calculated for clinopyroxenes from the massive lavas (1161 ± 34 °C) (Table S5).

5.2. Origin of Clinopyroxene Zoning

Clinopyroxene phenocrysts of variolitic and massive lavas exhibited similar zoning patterns, but were abundant to different extents. The massive lavas contained the lowest abundances of clinopyroxene phenocrysts, and the most abundant zoning pattern was HP clinopyroxenes, whereas the zoned clinopyroxenes were rarely recognized. In contrast, the variolitic lavas contained greater proportions of clinopyroxenes dominated by NZ and HP zoning patterns. Moreover, the OZ phenocrysts were recognized only in the variolitic lavas and not detected in the massive lavas. The variable proportions of the clinopyroxenes with different zoning patterns in the massive and variolitic lavas suggest that the melts that formed these rocks experienced different crystallization histories.

HP clinopyroxenes in the massive lavas are characterized by high Mg# and Cr₂O₃ contents gradually decreasing from the center to the margins (Figure 3a,f and Figure 4), with low REE content. The central parts of HP clinopyroxenes in the massive lavas are likely to crystallize from the most primitive mafic melt. Moreover, the margins of HP clinopyroxenes in the massive lavas were determined to be in equilibrium with their host whole-rock composition (Figure 7), and could be interpreted as autocrysts crystallized from a melt. Since the HP clinopyroxene phenocrysts represented the most abundant zoning pattern in the massive lavas, it can be assumed that the crystallization of the massive lavas mainly involved crystallization in a closed system or in a system with suppressed magma mixing. HP clinopyroxenes were also recognized in the variolitic lavas, where they exhibited similar compositional variations but lower Mg# and Cr₂O₃ contents.

Normal zoning in clinopyroxenes from the variolitic and massive lavas is defined by a decrease in Mg# and Cr₂O₃ contents coupled with an increase in TiO₂ and REE contents from the cores to rims (Figure 4, Table 1). It is noteworthy that the NZ cores were characterized by positive Nb anomalies in contrast to the NZ rims, which exhibited negative Nb anomalies. Positive Nb anomalies are typical for the most primitive picobasalts of Suisaari Fm and Zaonega Fm [33], which is interpreted [33] to be an indicator of the uncontaminated character of melts produced these rocks. High Mg# and positive Nb anomalies of the NZ cores suggest crystallization from the primitive melt with a composition similar to the high-Mg picobasalts from the Suisaari Fm. Based on their textural features, two types of NZ clinopyroxenes characterized by similar compositional variations were recognized in the variolitic and massive lavas. Notably, NZ Type I clinopyroxenes were abundant and NZ Type II was rarely detected in the variolitic and massive lavas. The cores of NZ Type I clinopyroxenes with high Mg# and low REE content were assumed to have crystallized from a less evolved melt. The cores exhibited no distinct resorption texture (Figure 3b,g) and the rim overgrowth was likely formed as a result of fractional crystallization—the process responsible for driving the geochemical evolution of the melt causes in subsequent rim growth, resulting in a distinct geochemically character compared to the rim/core. In contrast, the NZ Type II clinopyroxenes had a separating resorption surface between the cores and rims (Figure 3c,h), suggesting it is unlikely that the overgrowth rims originated due to fractional crystallization. The plausible explanation for this zoning pattern is that the core was a fragment of clinopyroxene crystallized in the more mafic magma. NZ Type II cores might be resorbed and subsequently overgrown by the rim with low Mg# during the mixing of evolved magma or convection from high-Mg to Mg-low zones of the magmatic system. NZ Type II pyroxenes exhibited relatively slight variations in core–rim composition, and NZ Type II cores had slightly low Mg# compared to NZ type I cores (Table 1), which originated from fractionation. Additionally, the compositions of NZ Type II cores were in equilibrium or close to equilibrium with the host rock composition. Based on this

data, we assume that convection is favored to produce NZ Type II clinopyroxenes, though we cannot exclude that NZ Type II formation involves magma mixing.

Reverse zoning and resorption textures are common in pyroxenes from various rocks [18,43,46], and are considered to record the open system processes, including magma mixing and contamination by host rocks [4,43]. Some of the clinopyroxenes in the variolitic lavas and a single crystal in the massive lavas exhibited reverse zoning that manifested as increasing Mg# from the core to rims, instead of Mg# decreasing (as is the case in normal zoning). Additionally, RZ clinopyroxenes are characterized by distinct disequilibrium features such as an overgrowth of rims on resorbed cores with dissolution surfaces. It is noteworthy that the RZ clinopyroxenes from the massive lavas were characterized by lower rim thicknesses and low resorption extents compared to those from the variolitic lavas (Figure 3d,i). However, reverse zoning can record not only variations of magma composition but also the variations of crystallization conditions (e.g., temperature or oxygen fugacity). If the reverse zoning reflects the variations of magma composition, there will be a correlation between Mg# and the other element contents [43].

The RZ clinopyroxenes from the variolitic and massive lavas displayed a positive correlation between Mg# and Cr₂O₃, and a negative correlation between Mg# and TiO₂, although this was better in the clinopyroxenes from the massive lavas ($R = 0.75$ and $R = -0.86$) than from the variolitic lavas ($R = 0.67$ and $R = -0.60$). These data provide additional evidence that reverse zoning leaves a record open magma system processes. The Mg-poor clinopyroxenes were assumed to crystallize from the more evolved melts, whereas the Mg-rich clinopyroxenes corresponded to the more primitive magmas. The similarity in REE and trace element distribution patterns between the cores and rims of the reverse-zoned clinopyroxenes (Figure 5e,f) precludes an origin involving crustal contamination in an open system. Therefore, the cores of RZ clinopyroxenes from the variolitic and massive lavas of the Yalguba Ridge were interpreted as antecrysts, suggesting that they can originate from magma mixing processes or convection within the magmatic system. In the case of RZ clinopyroxenes from variolitic lavas, magma mixing processes are favored, since convection is unlikely to produce such strong variation in the core–rim composition. Therefore, the cores of RZ clinopyroxenes are assumed to have crystallized from an early batch of magma during the magma mixing processes, revealing an evolved magma composition with low Mg# and Cr₂O₃ contents and high REE content, while the rims corresponded to a more primitive melt. In contrast, the RZ clinopyroxenes from the massive lavas exhibited less pronounced differences in core–rim composition and were determined to be close to equilibrium with the host's whole-rock composition (Figure 7), meaning they are likely to have been produced by convection in a closed system triggered by injection of high-Mg magma.

Previous studies [12,43,47] have shown that oscillatory zoning of minerals might be caused by the kinetics of crystal growth or magma processes such as magma mixing or convection. If the banding of oscillatory zoning is fine (<15 μm), it is thought to be kinetically controlled, and if the banding is coarse then oscillatory zoning reflects the compositional variations in the magma due to dynamic magmatic processes [43]. Oscillatory zoning was detected only for the clinopyroxenes from the variolitic lavas of the Yalguba Ridge, and was defined by a Mg-poor core, a relatively Mg-rich mantle, and a Mg-poor rim (Figure 4). Oscillatory zoning is characterized by the band widths ranging from 15 to 30 μm, suggesting magma composition variations. In general, there are two possibilities of oscillatory zoning in open magmatic systems, including repeated chamber replenishment events and crystal convection. OZ clinopyroxenes from the variolitic lavas had rounded cores with resorption features (Figure 3e,j) surrounded by euhedral mantles and rims with sharp boundaries. Moreover, the cores exhibited a significant chemical disequilibrium with the whole-rock host composition, whereas the mantles and rims were closer to equilibrium with some rim compositions with chemical equilibria (Figure 7). The cores of OZ clinopyroxenes were assumed to be antecrysts, with the core-mantle zone mainly reflecting changes in magma composition due to magma mixing, whereas the rims were likely produced by overgrowth on the mantle during fractionation processes. Similar to the RZ clinopyroxenes, Mg-poor

cores of the OZ clinopyroxenes were attributed to crystallization from evolved magma, whereas the Mg-rich bands corresponded to crystallization from primitive magma.

Zoned clinopyroxenes in the variolitic and massive lavas exhibited similarity in REE and trace element patterns (Figure 5). The cores and rims of zoned and unzoned clinopyroxenes exhibited similar compositional features such as convex upward REE distribution patterns with minor negative Eu anomalies and depletion in HFSE elements. The data suggest the clinopyroxenes in both variolitic and massive lavas originated from similar primary melts, probably a single magmatic source. However, the variations in texture, zoning, and composition of clinopyroxene phenocrysts between the variolitic and massive lavas indicate that the differentiation processes operated to different extents in the magma system. Though at the early stage clinopyroxenes from the variolitic and massive lavas crystallized from similar primary melts, their subsequent magmatic evolution significantly differed between the variolitic and massive lavas. The obtained data suggest that the crystallization of clinopyroxenes, which caused the different zonation patterns in the massive lavas, mainly involved fractionation in a closed magmatic system, whereas the crystallization of the variolitic lavas was determined by processes in an open magmatic system. Additional support for this conclusion comes from the CSD analysis of the clinopyroxenes in the variolitic and massive lavas.

It has been demonstrated [38,39] that CSD curves would be linear if the crystal growth were defined by homogeneous nucleation increasing exponentially with time in an open system corresponding to fractional crystallization. Kinked CSD curves likely reveal more complex crystallization resulting from various processes such as mixing, mechanical sorting, or Ostwald ripening [38,39]. CSD curves of clinopyroxenes from variolitic lavas are characterized by kinked CSD curves with a concave-upward curvature at sizes larger than 120 μm , which indicate the accumulation of a population of larger clinopyroxenes due to magma mixing in an open system (Figure 6). Clinopyroxene from the massive lavas exhibited mainly linear CSD curves, indicating that fractional crystallization was the dominant process. The concave-downward CSD curve observed for sizes smaller than 20 μm might have corresponded to Ostwald ripening, which involves the growth of large grains at the expense of small grains. The obtained CSD data for the variolitic and massive lavas coincide with the results of texture and zoning studies of the clinopyroxene phenocrysts, which suggest different crystallization histories for the variolitic and massive lavas.

5.3. Petrological Model and Conclusions

The present study of geochemistry and texture for the clinopyroxene phenocrysts from the Yalguba Ridge reveals that the variolitic and massive lavas are likely to have originated from a melt with a $\text{Mg\#} = 0.60\text{--}0.68$, which could be close in composition to the most primitive picobasalts of Suisaari Fm [33]. The supposed primary melt experienced variable extents of differentiation, including both closed and open system processes. The low amount of zoned clinopyroxene phenocrysts and the linear CSD curve suggest that crystallization of the massive lavas is likely to occur in a closed system or magmatic system with a suppressed accumulation of clinopyroxene antecrysts due to the magma recharge. The variolitic lavas of the Yalguba Ridge have a more complicated evolution history. A wide variety of clinopyroxene zoning patterns and kinked CSD curves prove that crystallization of the variolitic lavas took place in an open system and involved magma mixing and crystal convection in addition to magma fractionation. The magmatic processes for the variolitic and massive lavas can be generalized into the stages illustrated in Figure 8.

Stage I is common for both variolitic and massive lavas, and it involves the crystallization of high-Mg ($\text{Mg\#} > 88$) cores of NZ clinopyroxenes from both of those lavas, as well as homogeneous clinopyroxenes from the massive lava and mantles of OZ clinopyroxenes from the variolitic lava, which crystallized from the most primitive melt. Chemical characteristics of these clinopyroxenes, including high Cr_2O_3 content, low REE content, depletion of HREE, and positive Nb anomalies, correspond to the specific features of picobasalts from Suisaari Fm [33]. However, although stage clinopyroxenes from

variolitic and massive lavas crystallized from a similar primary magma, their subsequent crystallization evolutions differed significantly.

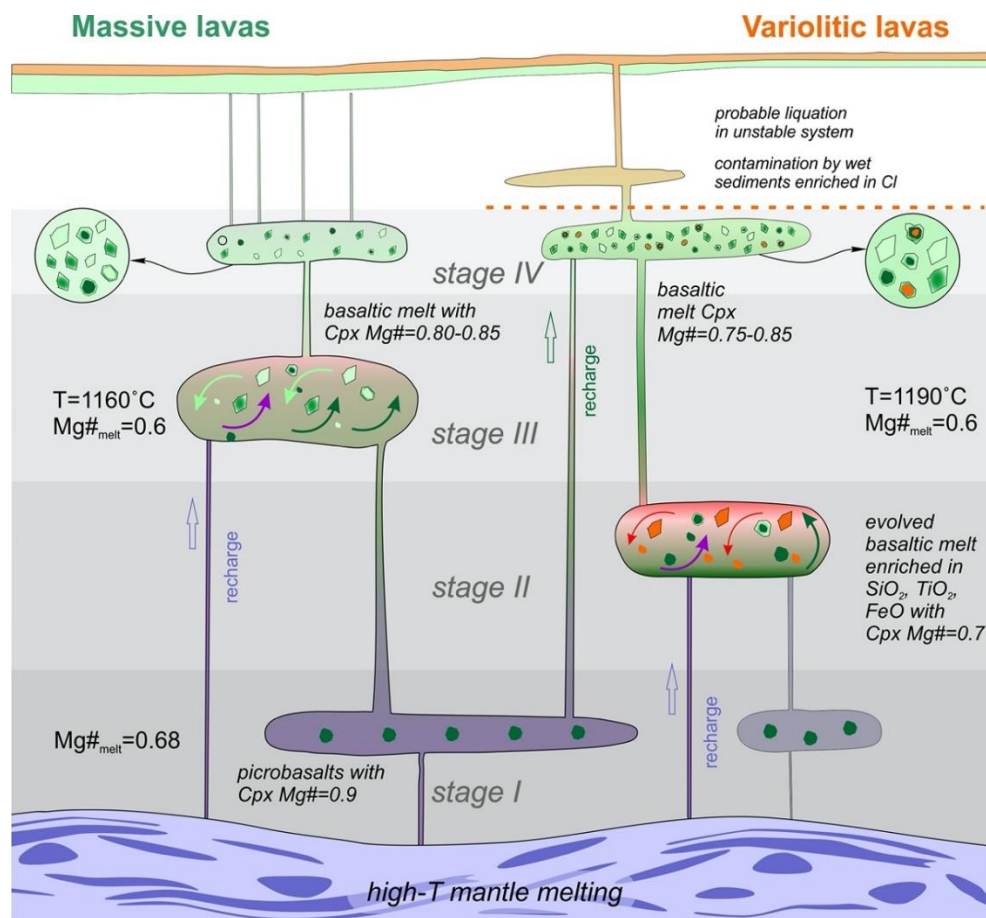


Figure 8. Schematic model of the evolution of the magmatic system for the Suisaarian massive and variolitic lavas based on the data for the clinopyroxene phenocrysts. Clinopyroxene types correspond to Table 1. The orange dotted line indicates a lower restriction for the generation of variolitic textures.

Stage II is specific to the crystallization of variolitic lavas in an open system, and involves the recharging of a primitive melt with a high Mg# and low REE content into a magma mush and/or transport of crystal cumulates, which could have caused a resorption of early clinopyroxene grains and produced the RZ and OZ clinopyroxenes in variolitic lavas (Figure 8). The cores of RZ and OZ clinopyroxenes with low Mg# = 0.70, high TiO₂ and REE content, and depletion of HFSE with negative Nb anomalies reflect the crystallization from the low-Mg evolved melt. Similar convex upward REE distribution patterns with minor negative Eu anomalies detected for the clinopyroxenes suggest that the low-Mg evolved melt originated from the fractionation of the primary magma. Depletion in HFSE with negative Nb anomalies might be assumed as an indicator of crustal contamination. The high-Mg composition of the mantle of the OZ clinopyroxenes shows the subsequent injection of primitive magma in an open system, which might additionally have produced the homogenous clinopyroxenes with high Mg#.

Stage III is similar for both variolitic and massive lavas, and involves crystal convection. Crystal convection in a recharged system in variolitic and massive lavas produces NZ Type II clinopyroxenes. Additionally, convection in a closed system is assumed to be responsible for the origin of the RZ clinopyroxenes in the massive lavas.

Stage IV involves fractionation of primary magma and produces homogenous and NZ Type I clinopyroxenes, as well as the RZ and OZ rims of both variolitic and massive lavas.

The obtained data reveal the different trends of the primary magma evolution in an open system for the variolitic lavas and a closed system for the massive lavas of the Yalguba Ridge, though they are likely to originate from a single primary magma.

The mechanism behind variolitic texture formation in volcanic rocks is a widely debated topic. The most widespread models proposed to explain this phenomenon include the liquation of basalt magma [19–23], or mixing of felsic and mafic magmas [24,25]. The obtained data for clinopyroxene phenocrysts in the variolitic lava of the Yalguba Ridge suggest that they crystallized from primary and evolved basaltic magmas derived from a single source. As such, it seems unlikely that the variolitic textures originated from the mixing of felsic and mafic magmas [24,25]. The liquation model [34] is based on whole-rock composition, which shows the differences in the REE and trace element distribution of globules and matrices in the variolitic lavas of the Yalguba Ridge (Figure 6). Moreover, two types of matrix composition were distinguished whereby one of the matrix types is characterized by a high content of the large-ion lithophile elements Rb, Ba and Sr and a depletion of HFSE elements, suggesting crustal contamination. Clinopyroxenes from variolitic lavas are characterized by a depletion of HFSE with negative Nb anomalies that might be assumed to be an indicator of crustal contamination. However, the obtained data are insufficient to provide arguments for and against the liquation model, and can only indicate potential time constraints on clinopyroxene phenocryst crystallization and liquation events. It might be assumed that clinopyroxene phenocrysts crystallized before the variolitic texture formation, since the similar textures and zoning patterns of clinopyroxene phenocrysts were recognized in both globules and matrices of the variolitic lavas. Therefore, the formation of variolitic textures on the lavas of the Yalguba Ridge might have occurred at the final stages of open system evolution and not have been recorded in the clinopyroxene chemistry.

The major and trace elements and the crystal size distribution of clinopyroxene phenocrysts hosted in the variolitic and massive lavas of the Yalguba Ridge (Suisaari Formation Onega Basin, Russia) led to the following conclusions:

1. Clinopyroxene phenocrysts in both variolitic and massive lavas originate from similar primary melts from a single magmatic source.
2. Crystallization of the massive lavas of the Yalguba Ridge mainly involves fractionation in a closed system, whereas the crystallization of the variolitic lava occurs in an open magmatic system and involves magma mixing and crystal convection.
3. The formation of variolitic textures in the lavas of the Yalguba Ridge might occur at the final stages of magmatic crystallization.

Supplementary Materials: The following are available online at <http://www.mdpi.com/2075-163X/10/5/434/s1>, Table S1: Whole-rock major (wt. %) and trace (ppm) element compositions of the variolitic lava [34] and massive lavas, Table S2: CSD data of clinopyroxene from the variolitic and massive lavas of the Yalguba Ridge, Table S3: Concentrations of major elements in representative clinopyroxene phenocrysts from the variolitic and massive lavas of the Yalguba Ridge, Table S4: SIM analysis data for representative clinopyroxene phenocrysts from the variolitic and massive lavas of the Yalguba Ridge, Table S5: KD (Fe-Mg) and crystallization temperatures calculated for clinopyroxenes from the variolitic and massive lavas using the clinopyroxene-only pressure independent thermometer [45].

Author Contributions: Conceptualization, S.A.S. and A.V.S.; investigation, S.A.S. and S.Y.C.; data curation, S.Y.C.; writing—original draft, S.Y.C.; writing—review and editing, S.A.S. and A.V.S.; visualization, S.Y.C. and A.V.S.; supervision, S.A.S. and A.V.S. All authors have read and agreed to the published version of the manuscript.

Funding: This research was funded by state assignment to Institute of Geology Karelian Research Centre RAS AAAA-A18-118020290085-4.

Acknowledgments: We are grateful to S.G. Simakin and E.V. Potapov (Yaroslavl Branch of the Physicotechnical Institute of RAS) for the SIMS study of clinopyroxenes. We thank two anonymous reviewers for their constructive comments, which helped us to improve the manuscript.

Conflicts of Interest: The authors declare no conflict of interest.

References

1. Nakada, S.; Bacon, C.R.; Gartner, A.E. Origin of phenocrysts and compositional diversity in Pre-Mazama rhyolitic lavas, Crater Lake, Oregon. *J. Petrol.* **1994**, *35*, 127–162. [[CrossRef](#)]
2. Nakagaw, M.; Wada, K.; Wood, C.P. Mixed magmas, mush chambers and eruption triggers: Evidence from zoned clinopyroxene phenocrysts in andesitic scoria from the 1995 eruptions of Ruapehu volcano, New Zealand. *J. Petrol.* **2002**, *43*, 2279–2303. [[CrossRef](#)]
3. Davidson, J.P.; Morgan, D.J.; Charlier, B.L.A.; Harlou, R.; Hora, J.M. Microsampling and isotopic analysis of igneous rocks: Implications for the study of magmatic systems. *Annu. Rev. Earth Planet. Sci.* **2007**, *35*, 273–311. [[CrossRef](#)]
4. Ginibre, C.; Worner, G.; Kronz, A. Crystal Zoning as an Archive for Magma Evolution. *Elements* **2007**, *3*, 261–266. [[CrossRef](#)]
5. Mollo, S.; Blundy, J.; Scarlato, P.; De Cristofaro, S.P.; Tecchiato, V.; Di Stefano, F.; Vetere, F.; Holtz, F.; Bachmann, O. An integrated P-T-H₂O-lattice strain model to quantify the role of clinopyroxene fractionation on REE+Y and HFSE patterns of mafic alkaline magmas: Application to eruptions at Mt. Etna. *Earth Sci. Rev.* **2018**, *185*, 32–56. [[CrossRef](#)]
6. Baziotis, I.; Xydous, S.; Asimow, P.D.; Mavrogonatos, C.; Flemetakis, S.; Klemme, S.; Berndt, J. The potential of phosphorus in clinopyroxene as a geospeedometer: Examples from mantle xenoliths. *Geochim. Cosmochim. Acta* **2019**, *266*, 307–331. [[CrossRef](#)]
7. Arndt, N.T.; Fleet, M.E. Stable and metastable pyroxene crystallization in layered komatiite lava flows. *Am. Mineral.* **1979**, *64*, 856–864.
8. Ubide, T.; Galé, C.; Arranz, E.; Lago, M.; Larrea, P. Clinopyroxene and amphibole crystal populations in a lamprophyre sill from the Catalanian Coastal Ranges (NE Spain): A record of magma history and a window to mineral-melt partitioning. *Lithos* **2014**, *184*, 225–242. [[CrossRef](#)]
9. Jankovics, M.É.; Taracsák, Z.; Dobosi, G.; Embey-Isztin, A.; Batki, A.; Harangi, S.; Hauzenbergere, C.A. Clinopyroxene with diverse origins in alkaline basalts from the western Pannonian Basin: Implications from trace element characteristics. *Lithos* **2016**, *262*, 120–134. [[CrossRef](#)]
10. Crossingham, T.J.; Ubide, T.; Vasconcelos, P.M.; Knesel, K.M.; Mallmann, G. Temporal constraints on magma generation and differentiation in a continental volcano: Buckland, eastern Australia. *Lithos* **2018**, *302*, 341–358. [[CrossRef](#)]
11. Ovung, T.N.; Ray, J.; Ghosh, B.; Koeber, C.; Topa, D.; Paul, M. Clinopyroxene composition of volcanics from the Manipur Ophiolite, Northeastern India: Implications to geodynamic setting. *Int. J. Earth Sci.* **2018**, *107*, 1215–1229. [[CrossRef](#)]
12. Wang, K.-Y.; Song, X.-Y.; Yi, J.-N.; Barnes, S.J.; She, Y.-W.; Zheng, W.-Q.; Schoneveld, L.E. Zoned orthopyroxenes in the Ni-Co sulfide ore-bearing Xiarihamu mafic-ultramafic intrusion in northern Tibetan Plateau, China: Implications for multiple magma replenishments. *Ore Geol. Rev.* **2019**, *113*, 103082. [[CrossRef](#)]
13. Miller, S.A.; Myers, M.; Fahnestock, M.F.; Bryce, J.G.; Blichert-Toft, J. Magma dynamics of ancient Mt. Etna inferred from clinopyroxene isotopic and trace element systematics. *Geochem. Perspect. Lett.* **2017**, *4*, 47–52. [[CrossRef](#)]
14. Mollo, S.; Ubide, T.; Di Stefano, F.; Nazzari, M.; Scarlato, D.P. Polybaric/polythermal magma transport and trace element partitioning recorded in single crystals: A case study of a zoned clinopyroxene from Mt. Etna. *Lithos* **2020**, *356–357*, 105382. [[CrossRef](#)]
15. Di Stefano, F.; Mollo, S.; Ubide, T.; Petrone, C.M.; Caulfield, J.; Scarlato, P.; Nazzari, M.; Andronico, D.; Del Bello, E. Mush cannibalism and disruption recorded by clinopyroxene phenocrysts at Stromboli volcano: New insights from recent 2003–2017 activity. *Lithos* **2020**, *360*, 105440. [[CrossRef](#)]
16. Leterrier, J.; Maury, R.C.; Thonon, P.; Girard, D.; Marchal, M. Clinopyroxene composition as a method of identification of the magmatic affinities of paleovolcanic series. *Earth Planet. Sci. Lett.* **1982**, *59*, 139–154. [[CrossRef](#)]
17. Nosova, A.A.; Sazonova, L.V.; Narkisova, V.V.; Simakin, S.G. Minor elements in clinopyroxene from Paleozoic Volcanics of the Tagil Island Arc in the Central Urals. *Geochemistry* **2002**, *40*, 219–233.

18. Liang, Y.; Deng, J.; Liu, X.; Wang, Q.; Qin, C.; Li, Y.; Yang, Y.; Zhou, M.; Jiang, J. Major and trace element, and Sr isotope compositions of clinopyroxene phenocrysts in mafic dykes on Jiaodong Peninsula, southeastern North China Craton: Insights into magma mixing and source metasomatism. *Lithos* **2018**, *302*, 480–495. [[CrossRef](#)]
19. Levinson-Lessing, F.Y. *Selected Manuscripts*; AN SSSR: Moscow, Russia, 1949; pp. 38–54.
20. Fergusson, J. Silicate Immiscibility in the Ancient Basalts of the Barberton Mountain Land, Transvaal. *Nat. Phys. Sci.* **1972**, *235*, 86–89. [[CrossRef](#)]
21. Gelin, L.; Brooks, C.; Trzcinski, W.E. Archean Variolites—Quenched Immiscible Liquids. *Can. J. Earth Sci.* **1976**, *13*, 210–230. [[CrossRef](#)]
22. Svetov, S.A. Liquefaction Differentiation in Basaltic Systems as Exemplified by the Suisarian Variolites of the Yalguba Range. *Geol. Ore Depos. Karelia* **2008**, *11*, 120–134.
23. Gudim, A.N.; Dubinina, E.O.; Nosova, A.A. Petrogenesis of Variolitic Lavas of the Onega Structure, Central Karelia. *Petrology* **2012**, *20*, 255–270. [[CrossRef](#)]
24. Krassivskaya, I.S.; Sharkov, E.V.; Bortnikov, N.S.; Chistyakov, A.V.; Trubkin, N.V.; Golovanova, T.I. Variolitic Lavas in the Axial Rift of the Mid-Atlantic Ridge and Their Origin (Sierra Leone Area, 6°18' N). *Petrology* **2010**, *18*, 263–277. [[CrossRef](#)]
25. Appel, P.W.U.; Polat, A.; Frei, R. Dacitic Ocelli in Mafic Lavas, 3.8–3.7 Ga Isua Greenstone Belt, West Greenland: Geochemical Evidence for Partial Melting of Oceanic Crust and Magma Mixing. *Chem. Geol.* **2009**, *258*, 105–124. [[CrossRef](#)]
26. Arndt, N.; Fowler, A.D. Textures in Komatiites and Variolitic Basalts. In *The Precambrian Earth: Temporal and Events*; Eriksson, P.G., Altermann, W., Nelson, D.R., Mueller, W.U., Catuneanu, O., Eds.; Elsevier: Amsterdam, The Netherlands, 2004; pp. 298–311.
27. Sandsta, N.R.; Robins, B.; Furnes, H.; de Wit, M. The Origin of Large Varioles in Flow Banded Pillow Lava from the Hooggenoeg Complex, Barberton Greenstone Belt, South Africa. *Contrib. Mineral. Petrol.* **2011**, *162*, 365–377. [[CrossRef](#)]
28. Hanski, E.J. Globular Ferropicritic Rocks at Pechenga, Kola Peninsula (Russia): Liquid Immiscibility Versus Alteration. *Lithos* **1993**, *29*, 197–216. [[CrossRef](#)]
29. Svetov, S.A.; Chazhengina, S.Y. Geological Phenomenon of Yalguba Ridge Variolite from F. Yu. Levinson-Lessing's Time until Today: Mineralogical and Geochemical Aspects. *Geol. Ore Depos.* **2018**, *60*, 547–558. [[CrossRef](#)]
30. Melezhik, V.A.; Hanski, E.J. The Pechenga Greenstone Belt. In *Reading the Archive of Earth's Oxygenation*; Melezhik, V.A., Prave, A.R., Fallick, A.E., Kump, L.R., Strauss, H., Lepland, A., Hanski, E.J., Eds.; Springer: Berlin/Heidelberg, Germany, 2013; pp. 289–385.
31. Narkisova, V.V. Petrology and geochemistry of igneous rocks in the OPB section. In *Paleoproterozoic Onega Structure: Geology, Tectonics, Structure, and Metallogeny*; Glushanin, L.V., Sharov, N.V., Shchiptsov, V.V., Eds.; KRS RAN: Petrozavodsk, Russia, 2011; pp. 195–208.
32. Kulikov, V.S.; Kulikova, V.V.; Lavrov, B.S.; Pisarevskii, S.A.; Pukhtel, I.S.; Sokolov, S.Y. *The Paleoproterozoic Suisarian Picrite–Basalt Complex in Karelia: Key Section and Petrology*; KNTs RAN: Petrozavodsk, Russia, 1999; pp. 34–58.
33. Puchtel, I.S.; Arndt, N.T.; Hofmann, A.W.; Haase, K.M.; Kröner, A.; Kulikov, V.S.; Kulikova, V.V.; Garbe-Schönberg, C.D.; Nemchin, A.A. Petrology of mafic lavas within the Onega plateau, central Karelia: Evidence for 2.0 Ga plume-related continental crustal growth in the Baltic Shield. *Contrib. Mineral. Petrol.* **1998**, *130*, 134–153. [[CrossRef](#)]
34. Svetov, S.A. Contamination as a factor for initiation of the magmatic liquefaction of basalt melts. *Litosfera* **2013**, *2*, 3–19.
35. Higgins, M.D. Measurement of crystal size distributions. *Am. Mineral.* **2000**, *85*, 1105–1116. [[CrossRef](#)]
36. Morimoto, N. Nomenclature of Pyroxenes. *Mineral. Petrol.* **1988**, *39*, 55–76. [[CrossRef](#)]
37. Sun, S.; McDonough, W.F. Chemical and isotopic systematics of oceanic basalts: Implications for mantle composition and processes. *Geol. Soc. Spec. Publ.* **1989**, *42*, 313–345. [[CrossRef](#)]
38. Marsh, B.D. On the interpretation of crystal size distributions in magmatic systems. *J. Petrol.* **1998**, *39*, 553–599. [[CrossRef](#)]
39. Jerram, D.A.; Martin, V.M. Understanding crystal populations and their significance through the magma plumbing system. *Geol. Soc. Spec. Publ.* **2008**, *304*, 133–148. [[CrossRef](#)]

40. Stepanova, A.V.; Samsonov, A.V.; Larionov, A.N. The final episode of the Mid-Paleoproterozoic magmatism in the Onega Basin: Data on dolerites in Zaonezhski peninsula. *Pros. Karel. Res. Cent. Ras* **2014**, *1*, 3–16.
41. Lubnina, N.V.; Stepanova, A.V.; Ernst, R.E.; Nilsson, M.; Söderlund, U. New U–Pb Baddeleyite age, and AMS and paleomagnetic data for dolerites in the Lake Onega region belonging to the 1.98–1.95 Ga regional Pechenga–Onega large igneous province. *GFF* **2016**, *138*, 54–78. [[CrossRef](#)]
42. Lubnina, N.V.; Pisarevsky, S.A.; Stepanova, A.V.; Bogdanova, S.V.; Sokolov, S.J. Fennoscandia before Nuna/Columbia: Paleomagnetism of 1.98–1.96 Ga mafic rocks of the Karelian Craton and paleogeographic implications. *Precambrian Res.* **2017**, *292*, 1–12. [[CrossRef](#)]
43. Streck, M.J. Mineral textures and zoning as evidence for open system processes. *Rev. Mineral. Geochem.* **2008**, *69*, 595–622. [[CrossRef](#)]
44. Putirka, K.D. Thermometers and Barometers for Volcanic Systems. *Rev. Mineral. Geochem.* **2008**, *69*, 61–120. [[CrossRef](#)]
45. Putirka, K.D.; Johnson, M.; Kinzler, R.; Longhi, J.; Walker, D. Thermobarometry of mafic igneous rocks based on clinopyroxene-liquid equilibria, 0–30 kbar. *Contrib Mineral Petrol.* **1996**, *123*, 92–108. [[CrossRef](#)]
46. Neumann, E.-R. Origin and evolution of the early magmatism in the Oslo Rift (Southeast Norway): Evidence from multiple generations of clinopyroxene. *Lithos* **2019**, *340–341*, 139–151. [[CrossRef](#)]
47. Elardo, S.M.; Shearer, C.K. Magma chamber dynamics recorded by oscillatory zoning in pyroxene and olivine phenocrysts in basaltic lunar meteorite Northwest Africa 032. *Am. Mineral.* **2014**, *99*, 355–368. [[CrossRef](#)]



© 2020 by the authors. Licensee MDPI, Basel, Switzerland. This article is an open access article distributed under the terms and conditions of the Creative Commons Attribution (CC BY) license (<http://creativecommons.org/licenses/by/4.0/>).